Physical characterization and origin of binary near-Earth asteroid (175706) 1996 FG$_3$[1]

Kevin J. Walsh

Southwest Research Institute, 1050 Walnut St. Suite 400, Boulder, CO, 80302, USA

`kwalsh@boulder.swri.edu`

Marco Delbo'

UNS-CNRS-Observatoire de la Côte d'Azur, BP 4229, 06304 Nice cedex 04, France

Michael Mueller

UNS-CNRS-Observatoire de la Côte d'Azur, BP 4229, 06304 Nice cedex 04, France
Low Energy Astrophysics, SRON, Postbox 800, 9700AV Groningen, Netherlands

Richard P. Binzel

Department of Earth, Atmospheric, and Planetary Sciences, Massachusetts Institute of Technology, Cambridge, Massachusetts 02139, USA

Francesca E. DeMeo

Department of Earth, Atmospheric, and Planetary Sciences, Massachusetts Institute of Technology, Cambridge, Massachusetts 02139, USA

ABSTRACT

The near-Earth asteroid (NEA) (175706) 1996 FG$_3$ is a particularly interesting spacecraft target: a binary asteroid with a low-Δv heliocentric orbit. The orbit of its satellite has provided valuable information about its mass density while its albedo and colors suggest it is primitive or part of the C-complex taxonomic grouping. We extend the physical characterization of this object with new observations of its emission at mid-Infrared (IR) wavelengths and with near-IR reflection spectroscopy. We derive an area-equivalent system diameter of 1.90 ± 0.28 km (corresponding to approximate component diameters of 1.83 km and 0.51 km, respectively) and a geometric albedo of 0.039 ± 0.012. (175706) 1996 FG$_3$ was previously classified as a C-type asteroid, though the combined 0.4–2.5 μm spectrum with thermal correction indicates classification as B-type;

both are consistent with the low measured albedo. Dynamical studies show that (175706) 1996 FG$_3$ has most probably originated in the inner main asteroid belt. Recent work has suggested the inner Main Belt (142) Polana family as the possible origin of another low-Δv B-type NEA, (101955) 1999 RQ$_{36}$. A similar origin for (175706) 1996 FG$_3$ would require delivery by the overlapping Jupiter 7:2 and Mars 5:9 mean motion resonances rather than the ν_6, and we find this to be a low probability, but possible, origin.

Subject headings: minor planets, asteroids: general

1.   Introduction

Among the ~ 37 known NEAs with satellites, (175706) 1996 FG$_3$ has a particularly low Δv value, making it an ideal target for a spacecraft mission (Perozzi et al. 2001; Christou 2003; Johnston et al. 2010). In fact, it is the baseline target of the ESA mission study Marco Polo-R (Barucci et al. 2011). (175706) 1996 FG$_3$, hereafter 1996 FG$_3$, is a prototype for the "asynchronous" NEA binaries. About 15% of all NEAs and small main belt asteroids (D < 10 km) are estimated to be such a binary (Pravec et al. 2006), and are characterized by a rapidly rotating primary (P < 4 h), a nearly spherical or oblate primary, and a moderately-sized secondary on a close orbit (Pravec et al. 2006).

1996 FG$_3$ was the first binary NEA for which eclipse events were detected in optical wavelengths (Pravec et al. 2000; Mottola & Lahulla 2000). From these and later observations, Scheirich & Pravec (2009) found the period of the mutual orbit to be 16.14 ± 0.01 hr, and a diameter ratio of $D_2/D_1 = 0.28^{+0.01}_{-0.02}$. A circular orbit is consistent with the data, but the preferred solution has $e = 0.10^{+0.12}_{-0.10}$ and semimajor axis $a \sim 3.4$ primary radii. The primary is an oblate ellipsoid with an axis ratio around $a/b \sim 1.2$, while the secondary is prolate with an axis ratio around 1.4. The spin period of the primary is 3.6 hr, that of the secondary is unknown. Scheirich & Pravec also find a mass density of $1.4^{+1.5}_{-0.6}$ g/cm^3 and an ecliptic latitude of the mutual spin axis of -84°.

The formation of these binaries points to a history of spin rate increase due to the thermal YORP effect, followed by re-shaping and mass-loss ending with a satellite in a

---

[1]Partially based on observations obtained at the European Southern Observatory (ESO, program ID 383.C-0179A). Observations were also obtained at the Infrared Telescope Facility, which is operated by the University of Hawaii under Cooperative Agreement no. NCC 5-538 with the National Aeronautics and Space Administration, Science Mission Directorate, Planetary Astronomy Program.

close orbit (Walsh et al. (2008); see also Scheeres (2007) work on fission of contact binary asteroids). This process demands a "rubble pile" or gravitational aggregate makeup, where bulk re-shaping is the cause for the ubiquitous oblate "top-shape" and equatorial ridge (see 1999 KW$_4$, Ostro et al. 2006). The process may end with preferential material migration from the poles of the primary towards the equator and also with general regolith depletion (Walsh et al. 2008; Delbo' et al. 2011).

Photometric observations determined the optical magnitude $H = 17.76 \pm 0.03$ and phase coefficient $G = -0.07 \pm 0.02$ (Pravec et al. 2006). Based on thermal observations (3.6 and 4.5 μm) using the "Warm Spitzer" space telescope, Mueller et al. (2011) find an area-equivalent diameter of this binary system of $1.8^{+0.6}_{-0.5}$ km and a geometric albedo of $p_V = 0.04^{+0.04}_{-0.02}$, consistent with a taxonomic classification in the C complex. It should be noted that their diameter and albedo values are based on an assumed color temperature (as opposed to a measured one), subjecting their results to significant systematic uncertainty. Wolters et al. (2011), observing at VLT, determined an effective diameter of 1.71$\pm$0.07 km and a geometric albedo of $p_V = 0.044 \pm 0.004$; furthermore they estimate the thermal inertia to be $\Gamma = 120 \pm 50$ J m^{-2} s$^{-0\,5}$ K^{-1}. Mueller et al. also studied the thermal history of 1996 FG$_3$ over its chaotic orbital evolution finding that it was likely (90%) heated above 482 K, possibly hot enough to induce thermal alteration of previously primitive surface material.

Pravec et al. (2000) and Mottola & Lahulla (2000) estimated that 1996 FG$_3$ is a C-type body from its broadband color indices and the steep phase dependence. The second phase of the SMASS survey's visible wavelength spectroscopy (0.44–0.92 micron) classified 1996 FG$_3$ as a C-type (Bus 1999), and when the spectroscopy of 1996 FG$_3$ was extended to $0.4 - 1.6$ μm by Binzel et al. (2001) 1996 FG$_3$ remained classified as a C-type. Recently, the taxonomic classification scheme of DeMeo et al. (2009) has leveraged data reaching 2.45 μm, though DeMeo et al. did not initially examine 1996 FG$_3$. De León et al. (2011) recently analyzed three spectra of 1996 FG$_3$, finding multiple acceptable taxonomic classifications; Ch, C, Xk and B-type.

In this study, we present new multi-wavelength observations, reflectance spectroscopy between 0.4 and 2.5 μm, and thermal-infrared photometry from 8–19 μm to extend the physical characterization of 1996 FG$_3$. We utilize dynamical modeling of main belt source regions for NEAs and analyze the possibility of the B-type Polana family as a source for 1996 FG$_3$.

2. Thermal-IR observations and thermal modeling

We measured the thermal emission of 1996 FG$_3$ from observations at mid-IR wavelengths (8–18.5 μm) and also obtained its visible reflected light. Combined with a suitable model of the surface thermal emission we determined its size and albedo; results are given in Sect. 2.3.

2.1. IRTF-MIRSI observations

We observed 1996 FG$_3$ on 1 May 2009 UT using the Mid-Infrared Spectrometer and Imager MIRSI (Deutsch et al. 2003; Kassis et al. 2008) on the NASA Infrared Telescope Facility (IRTF) on Mauna Kea, Hawaii. We used photometric filters centered at 8.7, 9.8, 11.6, and 18.4 μm with spectral bandwidths just short of $\sim 10\%$. A standard four-point chop-nod pattern was used to remove background flux. The night was clear with no perceptible clouds, and the atmospheric humidity decreased from $\sim 30\%$ to $\sim 6\%$. The Cohen et al. (1995) flux calibrator α Hya was observed before and after the target at very similar airmass. A second Cohen et al. (1995) standard, α Boo, was observed afterwards for cross-checks on the flux calibration. The IRTF IDL library[2] was used to coadd data as needed and to remove known instrument artifacts. Raw signal counts were derived using standard synthetic aperture procedures. Flux calibration factors and atmospheric extinction coefficients for each filter were derived from the observations of α Hya. Analyzing the calibrator observations (including α Boo) we reproduce their Cohen et al. (1995) fluxes to within 1% for N-band fluxes, and to within 4% for Q-band (18.4 μm). Color corrections to asteroid fluxes are expected to be at the percent level and were not applied. Final MIRSI fluxes are given in Table 1.

In the N-band filters, we typically performed one or two back-to-back repeat observations to ascertain repeatability, which was within 10%. No such variation is seen in repeat observations of the flux calibrators, likely due to fluctuations in the background level. Our observations cover a fraction of the 3.6 hr rotation period (with a low-amplitude lightcurve), and given the reported repeatability, no lightcurve correction was attempted.

MIRSI observations were interspersed with V-band photometry observations using the optical CCD *Apogee*, which was calibrated against observations of Landolt (1973) standard SA 101-57. Due to the proximity in airmass (<0.05), extinction correction is not critical; we assumed an extinction coefficient of 0.12 mag/airmass. The 12 measured V magnitudes are constant within the photometric uncertainty of typically 0.15 mag per data point, no

---

[2]http://irtfweb.ifa.hawaii.edu/~elv/mirsi_steps.txt

indication of a V-band lightcurve was detected. The average V mag measured is 16.94, in excellent agreement with the expected V magnitude of 16.94 ± 0.13 for lightcurve average (based upon $H = 17.76 \pm 0.03$, $G = -0.07 \pm 0.02$, Pravec et al. 2006).

2.2. VLT-VISIR observations

Independent thermal-IR observations of 1996 FG_3 were obtained on 2 May 2009 UT using the VLT Imager and Spectrometer for mid Infrared (VISIR; Lagage et al. 2004) installed at the 8.2m VLT Melipal telescope of the European Southern Observatory (ESO), Cerro Paranal, Chile. Photometric observations were carried out through narrow-band filters centered at 8.59, 11.88 and 18.72 μm. The observation design was largely analogous to that of our MIRSI observations (see Sect. 2.1). The Cohen et al. (1995, 1999) standard star HD93813 was observed at an airmass very similar to that of the science target and used for absolute flux calibration.[3] Data were reduced as described above, except in the case of the PAH_2 filter centered at 11.88 μm, where coadded asteroid data appeared "smeared." In order to correct for the flux lost outside the nominal 10-pixel-radius synthetic aperture, the nominal 11.88 μm flux was increased by a factor of 13%, derived using the growth curve method (Howell 1989). To test the importance of this approximation we fit the data without this point, and also with this point with a 10% and 20% uncertainty, finding at most a 3% change in diameter and no change in η. See Table 2 for final fluxes.

2.3. Diameter and albedo results

We used the Near-Earth Asteroid Thermal Model (NEATM, Harris 1998)[4] to fit the thermal fluxes reported in Table 1 and 2. NEATM fluxes are calculated by integrating the Planck function over the visible and illuminated part of the surface of a spherical model asteroid. The surface is assumed to be in instantaneous thermal equilibrium with the absorbed sunlight, where temperatures across the surface can be rescaled to match the spectral energy distribution of the observed fluxes. This temperature rescaling is expressed in terms of a dimensionless "beaming parameter" η such that $T^4 \propto \eta$. Note that our observations do not spatially resolve 1996 FG_3. Thus, the NEATM-derived diameter D is that of a sphere with the combined cross-sectional area of the two components. The (area-equivalent) component

---

[3]see http://www.eso.org/sci/facilities/paranal/instruments/visir/tools/zerop_cohen_Jy.txt

[4]See also Delbo' & Harris (2002) for an introduction and overview.

diameters D_1 and D_2 are related to D via $D_1{}^2 + D_2{}^2 = D^2$.

In order to determine the statistical uncertainty in the fit parameters of the NEATM D, p_V, and η, we performed a Monte-Carlo analysis analogous to that described by Mueller et al. (2007) in which 300 random flux sets are generated, normally distributed about the measured data. The median of the Monte-Carlo results is adopted as the nominal result with asymmetric error bars encompassing the central 68.2% of the results (see Mueller et al. 2011, for a more detailed discussion of this method).

This Monte-Carlo analysis was performed for each dataset (see Tables 1 and 2) and for their combination—note that the observation geometry is essentially identical between the two nights; the corresponding change in expected flux is of the order of 1.6%. Given the apparent discrepancy between the Q-band fluxes measured during the two nights (see below), we repeat this analysis for all datasets minus Q-band fluxes. All results along with Monte-Carlo uncertainties are given in Table 3. The data are plotted in Figure 1 along with the adopted best-fit model curve.

The true uncertainties in D and p_V are dominated by the systematic uncertainty inherent in the NEATM, which is conventionally estimated to be 15% in D and 30% in p_V (Harris 2006). In the (exceptional) case of 1996 FG$_3$, the uncertainty in H does not contribute significantly to the error budget. Our results from the different datasets are in excellent mutual agreement; in particular, the Q-band fluxes are largely inconsequential for our purposes. We adopt the average of the first six lines in Table 3 as our final result, including the systematic D and p_V uncertainty; the adopted η uncertainty is the scatter between the six datasets: $D = 1.90 \pm 0.28$ km, $p_V = 0.039 \pm 0.012$, and $\eta = 1.61 \pm 0.08$. Using the known diameter ratio of $D_2/D_1 = 0.28^{+0.01}_{-0.02}$ (Scheirich & Pravec 2009), the corresponding (area-equivalent) component diameters are $D_1 = 1.83 \pm 0.28$ km and $D_2 = 0.51 \pm 0.08$ km.

Our results are in excellent agreement with those reported by Mueller et al. (2011) based on Warm-Spitzer observations ($D = 1.8^{+0.6}_{-0.5}$ km and $p_V = 0.04^{+0.04}_{-0.02}$) and with those reported by Wolters et al. (2011) ($D = 1.71 \pm 0.07$ km, $p_V = 0.044 \pm 0.004$, and $\eta = 1.15$). Note that Wolters et al.'s observations took place at a significantly lower phase angle (11.7°) than ours (67.4°), hence the difference in best-fit η values is consistent with expectations (Delbo' et al. 2007). Mueller et al. (2011) did not constrain η, but assumed a value. The good mutual diameter agreement of these three studies therefore provides independent support for the assumptions made by Mueller et al. (2011).

3.   Visible-Near-IR reflectance and 1996 FG$_3$'s main-belt origin

As part of the MIT-UH-IRTF Joint Campaign for NEO Spectral Reconnaissance the reflectance of 1996 FG$_3$ was measured between 0.8 and 2.5 μm. In Figure 2 the visible reflectance from the SMASS survey is combined with the near-IR to provide reflectance from 0.37–2.5 μm (Binzel et al. 2004). The spectrum presented was measured on 30 March 2009. A total integration time of 2880 seconds was obtained during a one-hour interval beginning at 11:17 UT. A nearby solar analog star, Landolt 105-76, was observed at similar airmass immediately following the asteroid measurements.

The 30 March 2009 spectrum of 1996 FG$_3$ does not yield a unique class, rather the allowable classes of C, Ch, or Xk type was determined by the online visible-near-IR taxonomy classifier based on the DeMeo visible near-IR taxonomy (DeMeo et al. 2009; De León et al. 2011). However, a B-type classification in the DeMeo taxonomy demands a negative slope to 2.45 μm, and in the spectrum a thermal tail is evident starting $\sim$2.0 μm (see Fig. 2). We fit the NEATM to the thermal tail of the SpeX data using the method described in Delbo' et al. (2011). A large range in p_V–η combinations fit the thermal tail well, though we use p_V=0.04, $\eta \sim 1.2$. The phase angle during the SpeX observations was $\sim 8°$, i.e., much lower than during our mid-IR photometric observations, hence such a low η is consistent with our expectations.

The thermally-corrected spectrum was classified as a B-type by the online classification system (DeMeo et al. 2009). De León et al. (2011) find that the 27 April 2009 spectrum also taken by the MIT-UH-IRTF campaign of lower SNR is classified as a B-type by the same online tool. However, their spectrum, taken at Telescopio Nazionale Galileo (TNG) on 9 January 2011, is labeled a Ch or Xk type. We move forward with a B-type classification, though naming a taxonomic type is less indicative of composition than an analysis of spectral features.   Therefore we provide a quantitative comparison and a qualitative interpretation of inferred spectral features.

The $\approx$ 50 km Main Belt asteroid (142) Polana is the largest member of a family proposed to have been the main-belt origin of B-type NEO 1999 RQ$_{36}$ (Campins et al. 2010), due in large part to its B-type spectrum. To quantify the similarity between these spectra we follow the χ^2 formulation used by De León et al. (2010) and Campins et al. (2010) between 0.475 and 1.925 μm with spacing of 0.0025 μm. Campins et al. (2010) found a $\chi^2 = 4.91$ when comparing 1999 RQ$_{36}$ with (142) Polana. Using a similar, but not exact, wavelength range we find a value $\chi^2 = 4.83$ for these two objects. 1996 FG$_3$ compared to 1999 RQ$_{36}$ and (142) Polana yield values of $\chi^2 = 1.09$ and 1.86, showing a strong similarity to both. The closest fit found by Campins et al. (2010) for 1999 RQ$_{36}$ and 27 main belt B-type asteroids was $\chi^2 = 1.33$, so its likeness to another B-type such as 1996 FG$_3$ is naturally greater than that

to the other main belt bodies in that study. Similarly, the match between 1996 FG_3 and (142) Polana is also closer than for 1999 RQ_{36} and (142) Polana. However, when comparing spectra via a χ^2 routine, features representing mineralogical differences can be marginalized in favor of bulk shape or slope.

There are subtle but clearly revealed differences between the three asteroids (Figure 2) that may allow differing mineralogical interpretations. The features near 1.2 and 2.0 μm for 1996 FG_3 are consistent with the presence of some olivine and some pyroxene, where the shallow depth of the features could be due to opaques. Note, however, that De León et al. (2011) rejects these two features due to the shape and location of the first band. This is an important disagreement, as our interpretation imply silicates, whereas De León et al. (2011) does not. The deeper 1.2 μm feature for Polana, with no feature at 2.0 μm is consistent with the presence of olivine (and perhaps opaques). Having spectral hints of olivine and pyroxene is possibly consistent with the spectral properties of ureilite meteorites (Cloutis et al. 2010), whereas the interpretation of De León et al. (2011) is more suggestive of carbonaceous chondrites (they suggest CM2). However, 1999 RQ_{36} is itself distinct from the others for its lack of 1 and 2 μm spectral features, which is more typical of carbonaceous chondrites.

De León et al. (2011) also made comparisons with meteorite spectra from the RELAB databse. Their TNG spectra was best fit by a combination of CM2 carbonaceous chondrites, and L4 and H5 ordinary chondrites. Their preferred match for the high-SNR MIT data was with a weakly shocked H4 ordinary chondrite.

4. Dynamical history and 1996 FG_3's main-belt origin

The chaotic nature of NEA orbital evolution makes it impossible to know the exact history for any given body. However, detailed orbital evolution modeling by Bottke et al. (2002) allows probabilistic estimates for Main Belt source regions to be made. The Bottke et al. work finds that the current orbit of 1996 FG_3 supports a 92% likelihood that it became an NEA after escaping the inner Main Belt via the ν_6 secular resonance[5].

The ν_6 marks the inner limit of the main asteroid belt and thus asteroids only reach this resonance by migrating inward from orbits with a larger semi-major axis ($a > 2.15$ AU). Similarly, this region is bounded at large semi-major axis by the 3:1 mean motion resonance

---

[5] This probability was determined using the 3-source NEO model, where 3 Main Belt sources are modeled as the parent populations for NEOs. This is the technique used for 1999 RQ_{36} by Campins et al. (2010).

(MMR) with Jupiter located at 2.5 AU. Thus, escape by the ν_6 resonance requires an initial semi-major axis range of $2.15 < a < 2.5$ AU, and inward migration. Escape by the ν_6 largely retains the inclination of the orbit so that the current 1.99° inclination is likely near its original inclination in the Main Belt.

A similar analysis has been done for the NEA 1999 RQ$_{36}$ where its orbital, physical and rotation properties were used to infer a parent family in the inner main belt. Its match with the (142) Polana family is due in large part to its classification as a B-type asteroid, and similarities in their visible/near-IR spectra. Dynamically, 1999 RQ$_{36}$ was found to have a 95% probability of coming from the inner belt via the ν_6 resonance, and has a low inclination of $i \sim 6.04°$. 1999 RQ$_{36}$ is in retrograde rotation, and also has a "top-shape" which has been found frequently among binary NEAs (Nolan et al. 2007; Harris et al. 2009).

Despite uncertainties in the Polana family's age, small members (H > 18.5) have already reached the ν_6 resonance by the Yarkovsky effect (Campins et al. 2010). The retrograde rotation of 1999 RQ$_{36}$ also indicates that its Yarkovsky drift is inward, allowing it to drift from the (142) Polana family towards the ν_6 resonance.

1996 FG$_3$ however, has H=17.76 and thus should not have had time to reach the ν_6 resonance by the Yarkovsky effect according to this estimate of the Polana family extent (Campins et al. 2010) (Note also that no definitive age is known for Polana due to its member's overlap with the Nysa family). However, it is possible for objects the size of 1996 FG$_3$ to reach the overlapping Jupiter 7:2 and the Mars 5:9 resonances located at a=2.2559-2.2569 AU and a=2.2542-2.2550 AU (Morbidelli & Nesvorny 1999; Bottke et al. 2007). This region of overlapping resonances is discussed in the Supplementary Material of Bottke et al. (2007), but its efficiency as a source is uncertain for objects of 2 km such as 1996 FG$_3$. Figure S6 of Bottke et al. (2007) shows roughly equal numbers of 5 km bodies jumping the resonance or getting trapped and excited.

Smaller objects will have higher Yarkovsky drift rates, likely lowering the fraction that get excited onto planet-crossing orbits. We tested the efficiency of resonance-crossing for ~ 2 km bodies drifting at their maximum Yarkovsky drift rates, which provides a lower limit. We used a modified version of `swift_rmvs` that applied a constant change in semi-major axis of -10^{-4} AU Myr^{-1} as estimated from Bottke et al. (2006) as an upper limit for its Yarkovsky drift rate at this size. We tested a set of 155 massless test particles initially located at $a \approx 2.26$ AU. The particles had initial e and i values similar to those of Polana, and 21 of the 155 particles had their eccentricities excited to Mars-crossing levels while crossing the resonance, and evolving onto Mars-crossing orbits. From here their evolution onto NEO orbits will be relatively rapid and leave them virtually indistinguishable from asteroids entering NEO-space via the ν_6 resonance.

The 21 particles excited out of the inner Main belt all had initial eccentricities above 0.15, pointing to the resonance's increasing effectiveness for higher e. The Polana family itself covers a range from e=0.13–0.17, even though (142) Polana itself has an e=0.136. Even with the conservative assumption of the maximum Yarkovsky drift rate for a D=2 km asteroid, approximately 10 % of the of family members this size would exit the inner Main Belt by the overlapping J7:2 and M5:9 resonances. Therefore, 1996 FG_3 could still have an origin with the Polana family as it fits the other major criteria used by Campins et al. (2010) to locate (142) Polana as a possible parent family of 1999 RQ_{36}: a B-type asteroid, a likely inner-Main Belt origin, low inclination, retrograde rotation. Making this study more general, to estimate the number of Polana members of this size in the NEO population, is challenging due to the uncertainties surrounding the exact size and age of the Polana family.

5.   Results and Conclusions

The findings of these observations and dynamical studies are;

1. 1996 FG_3 has a diameter of 1.90±0.28 km and a geometric albedo of $p_V = 0.039$±0.012,

2. Available data do not uniquely place 1996 FG_3 into a single taxonomic class; the best data (highest SNR) with a thermal flux correction applied, are most consistent with the B-class,

3. 1996 FG_3 is likely (92%) to have come from the inner Main Belt via the ν_6 resonance, though it could have escaped by the overlapping J7:2/M5:9 resonances located at 2.255 AU.

Together, these results provide a much better picture of the origin of 1996 FG_3 and raise some tantalizing questions about its relation to the NEA 1999 RQ_{36}, another ideal space mission target and primary target of NASA's OSIRIS-REx sample return mission (Lauretta et al. 2010).

Delbo' et al. (2011) studied the thermal properties of binary NEAs which have been observed in the thermal-IR, finding that statistically elevated η values, used as a proxy for thermal inertia, pointed to cooler surfaces than non-binary NEAs. This was interpreted in terms of regolith loss during the binary-formation process. Here, 1996 FG_3 was fit with an η of 1.61 ± 0.08. The large phase angle $\sim 68°$ makes this less constraining, but the values are elevated compared to the sample presented in Delbo' et al. (2011). Wolters et al. (2011) obtained $\eta \sim 1.15$ at a phase angle of 11.7°. Taken together, the available thermal-IR

data should enable a robust determination of the thermal inertia; that will be discussed, however, in a forthcoming paper (Mueller et al., 2012, in preparation). In comparison, the thermal inertia of 1999 RQ$_{36}$ has been estimated to be around 600 J m^{-2} s$^{-0\,5}$ K^{-1} (Emery et al. 2010). Based on the correlation between thermal inertia and object size found by Delbo' et al. (2007), and using $D \sim 0.58$ km (Nolan et al. 2007), a thermal inertia around 400 J m^{-2} s$^{-0\,5}$ K^{-1} would be expected, somewhat lower than measured. While 1999 RQ$_{36}$ is not known to be a binary, its radar shape, oblate with a possible equatorial ridge, is suggestive of YORP spinup and reshaping. Like in the case of YORP binaries, this could lead to an elevated thermal inertia such as that given by Emery et al. (2010).

1996 FG$_3$ and 1999 RQ$_{36}$ share many physical properties and possibly a similar dynamical history. As shown in Section 3, there is some uncertainty about the precise taxonomy for 1996 FG$_3$, though its spectra is qualitatively similar, with a negative slope from 0.5-2.0 μm, to that of 1999 RQ$_{36}$. The features for 1996 FG$_3$ at 1.2 and 2.0 μm are an important distinction between 1996 FG$_3$ and 1999 RQ$_{36}$. If these features are indicative of silicates then 1996 FG$_3$ may have more similarities with ureilites than with carbonaceous chondrites. In contrast, the featureless spectra of 1999 RQ$_{36}$ is suggestive of properties similar to carbonaceous chondrites, with CM typically cited as close matches for "B-types" depending on the level of thermal processing De León et al. (2011); Clark et al. (2010); Hiroi et al. (1996).

It is important to note that Jenniskens et al. (2009) obtained a low signal-to-noise visible spectrum of asteroid 2008 TC$_3$ prior to its Earth impact and subsequent recovery as the Almahata Sitta meteorite. While their initial interpretation of this spectrum suggested F- or B-type classification in the system of Tholen (1989), that classification is not confirmed with the addition of near-infrared spectrum of a Almahata Sitta meteorite presented by Jenniskens et al. (2010) and Hiroi et al. (2010). While a composite average spectrum of different stones of Almahata Sitta reproduces the 2008 TC$_3$ visible spectrum, none of the measured lab spectra matches the B-class (or any asteroid class defined over the full spectral range defined by DeMeo et al. (2009)).

We also note that the F-class itself diverges (fails to exist) for objects whose spectra are extended from the visible wavelengths to the near-infrared. As discussed by DeMeo et al. (2009), objects that are spectrally similar over visible wavelengths and satisfy the Tholen (1989) definition of the "F-class" diverge from one another as their spectra are extended into the near-infrared. Thus at present, the visible plus near-infrared spectrum of the Almahata Sitta meteorite spectrum fits into no asteroid taxonomy class and closely resembles no other currently measured spectrum of any asteroid.

Jenniskens et al. (2010) also pursued a parent source family for 2008 TC$_3$ similar to the dynamical work of Campins et al. (2010) for 1999 RQ$_{36}$. The most probable source region

was found to be the inner main asteroid belt via the ν_6 resonance ($\sim$80% probability): the same source region as 1996 FG$_3$ and 1999 RQ$_{36}$. Jenniskens et al. (2010) speculated the (142) Polana family as a source for 2008 TC$_3$. However the jumbled asteroid-meteorite link for the spectrum of 2008 TC$_3$ renders any further connection beyond the scope of this work.

Thus the implication of this study are that two prime space-mission targets, 1999 RQ$_{36}$ and 1996 FG$_3$ share similar taxonomies, spectra and possibly even rotation history (YORP-spinup). Linking them to the same parent family in the inner-main belt, the Polana family, is highly speculative as 1996 FG$_3$ would have had to escape by a minor resonance rather than ν_6. However, it cannot be ruled out entirely as we have shown that the J7:2/M5:9 resonances can push asteroids these size onto Mars-crossing orbits and on the path to near-Earth orbits.

REFERENCES

Barucci, M. A., Cheng, A. F., Michel, P., Benner, L.A.M., Binzel, R.P., Bland, P.A., Bonhardt, H., Brucato, J.R., Campo, A., Bagatin; Cerroni, P., Dotto, E., Fitzsimmons, A., Franchi, I.A., Green, S.F., Lara, L.-M., Licandro, J., Marty, B., Muinonen, K., Nathues, A., Oberst, J., Rivkin, A.S., Robert, F., Saladino, R., Trigo-Rodriguez, J.M., Ulamec, S., & Zolensky, M., 2011, submitted

Binzel, R. P., Harris, A. W., Bus, S. J., & Burbine, T. H. 2001, Icarus, 151, 139

Binzel, R. P., Rivkin, A. S., Stuart, J. S., Harris, A. W., Bus, S. J., & Burbine, T. H. 2004, Icarus, 170, 259

Bottke, W. F., Morbidelli, A., Jedicke, R., Petit, J.-M., Levison, H. F., Michel, P., & Metcalfe, T. S. 2002, Icarus, 156, 399

Bottke, W. F., Jr., Vokrouhlický, D., Rubincam, D. P., & Nesvorný, D. 2006, AREPS, 34, 157

Bottke, W. F., Vokrouhlický, D., & Nesvorný, D. 2007, Nature, 449, 48

Bus, S. J. 1999, Ph.D. Thesis,

Campins, H., Morbidelli, A., Tsiganis, K., de León, J., Licandro, J., & Lauretta, D. 2010, ApJ, 721, L53

Campins, H., et al. 2010, Nature, 464, 1320

Christou, A. A., 2003, Planet. Space Sci., 51, 221

Clark, B. E., et al. 2010, Journal of Geophysical Research (Planets), 115, 6005

Cloutis, E. A., Hudon, P., Romanek, C. S., Bishop, J. L., Reddy, V., Gaffey, M. J., & Hardersen, P. S. 2010, Meteoritics and Planetary Science, 45, 1668

Cohen, M., Witteborn, F.C., Walker, R.G., Bregman, J.D., Wooden, D.H., 1995, AJ, 110, 275

Cohen, M., Walker, R. G., Carter, B., Hammersley, P., Kidger, M., & Noguchi, K. 1999, AJ, 117, 1864

De León, J., Campins, H., Tsiganis, K., Morbidelli, A., & Licandro, J. 2010, A&A, 513, A26

De León, J., Mothé-Diniz, T., Licandro, J., Pinilla-Alonso, N., & Campins, H. 2011, A&A530, L12

Delbo', M., & Harris, A. W. 2002, Meteoritics and Planetary Science, 37, 1929

Delbo', M., Dell'Oro, A., Harris, A. W., Mottola, S., & Mueller, M. 2007, Icarus, 190, 236

Delbo', M., Walsh, K., Mueller, M., Harris, A. W., & Howell, E. S. 2011, Icarus, 212, 138

DeMeo, F. E., Binzel, R. P., Slivan, S. M., & Bus, S. J. 2009, Icarus, 202, 160

Deutsch, L.K., Hora, J.L., Adams, J.D., & Kassis, M., 2003, Proc. SPIE, 4841, 106

Emery, J. P., Fernández, Y. R., Kelley, M. S., Hergenrother, C., Ziffer, J., Lauretta, D. S., Drake, M. J., & Campins, H. 2010, Lunar and Planetary Institute Science Conference Abstracts, 41, 2282

Harris, A.W. 1998, Icarus, 131, 291

Harris, A. W., 2006, Proceedings IAU Symposium No. 229 (ACM 2005; D. Lazzaro, S. Ferraz-Mello, J. A. Fernández, eds.), pp 449-463.

Harris, A. W., Fahnestock, E. G., & Pravec, P. 2009, Icarus, 199, 310

Hiroi, T., Zolensky, M. E., Pieters, C. M., & Lipschutz, M. E. 1996, Meteoritics and Planetary Science, 31, 321

Hiroi, T., Jenniskens, P., Bishop, J. L., Shatir, T. S. M., Kudoda, A. M., & Shaddad, M. H. 2010, Meteoritics and Planetary Science, 45, 1836

Howell, S. B. 1989, PASP, 101, 616

Hsieh, H. H., & Jewitt, D. 2006, Science, 312, 561

Jenniskens, P., et al. 2009, Nature, 458, 485

Jenniskens, P., et al. 2010, Meteoritics and Planetary Science, 45, 1590

Johnston, W. R., Richardson, D. C., & Walsh, K. J. 2010, NASA Planetary Data System, 128,

Kassis, M., Adams, J.D., Hora, J.L., Deutsch, L.K., & Tollestrup, E.V., 2008, PASP, 120, 1271

Lagage, P. O., and 25 colleagues 2004, The Messenger, 117, 12-16.

Landolt, A.U. 1973, AJ, 78, 959–981.

Lauretta, D. S., et al. 2010, Meteoritics and Planetary Science Supplement, 73, 5153

Licandro, J., Campins, H., Mothé-Diniz, T., Pinilla-Alonso, N., & de León, J. 2007, A&A, 461, 751

Morbidelli, A. & Nesvorny, D. 1999, Icarus, 139, 295

Mothé-Diniz, T., Roig, F., & Carvano, J. M. 2005, Icarus, 174, 54

Mottola, S., Lahulla, F., 2000, Icarus, 146, 556

Mueller, M., Harris, A.W., & Fitzsimmons, A., 2007, Icarus, 187, 611

Mueller, M. and 16 coauthors, 2011, AJ, 141, 109

Nolan, M. C., Magri, C., Ostro, S. J., Benner, L. A., Giorgini, J. D., Howell, E. S., & Hudson, R. S. 2007, Bulletin of the American Astronomical Society, 38, 433

Ostro, S. J., et al. 2006, Science, 314, 1276

Perozzi, E., Rossi, A & G. B. Valsecchi, 2001, Planet. Space Sci., 49, 3

Pravec, P. et al. 2000, Icarus, 146, 190–203.

Pravec, P., and 56 colleagues 2006, Icarus, 181, 63

Rayner, J. T., Toomey, D. W., Onaka, P. M., Denault, A. J., Stahlberger, W. E., Vacca, W. D., Cushing, M. C., & Wang, S. 2003, PASP, 115, 362

Rivkin, A. S., & Emery, J. P. 2010, Nature, 464, 1322

Scheeres, D. J. 2007, Icarus, 189, 370

Scheirich, P. and P. Pravec, 2009, Icarus 200, 531–547.

Tholen, D. J. 1989, Asteroids II, 1139

Walsh, K. J., Richardson, D.C., & P. Michel, 2008, Nature, 454, 188

Wolters, S. D., Rozitis, B., Duddy, S. R., Lowry, S. C., Green, S. F., Snodgrass, C., Hainaut O. R. & P. Weissman, 2011, MNRAS, 418, 1246–1275
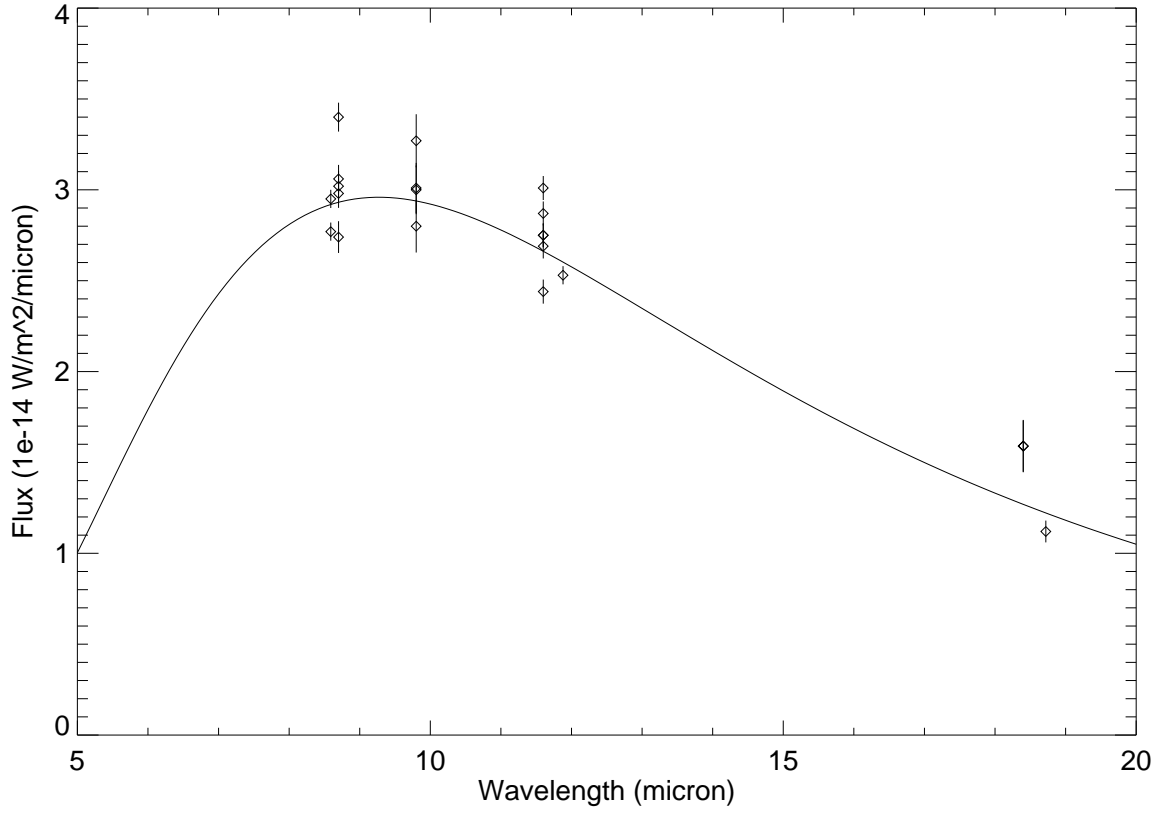
Fig. 1.— Thermal-IR data of 1996 FG$_3$ (see Tables 1 and 2) and NEATM model curve using the adopted parameters from Table 3.
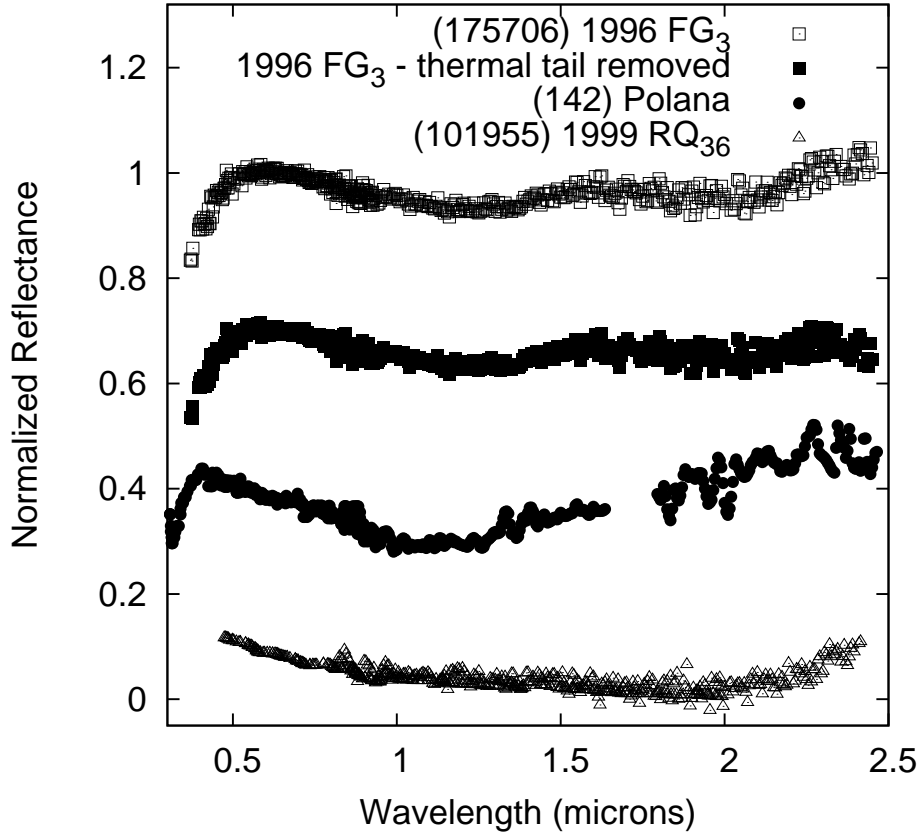
Fig. 2.— Visible-near-IR spectral reflectance from 0.4–2.5 μm for 1996 FG$_3$, 1996 FG$_3$ with the thermal tail removed, (142) Polana and 1999 RQ$_{36}$ (B. Clark et al. 2011 submitted).
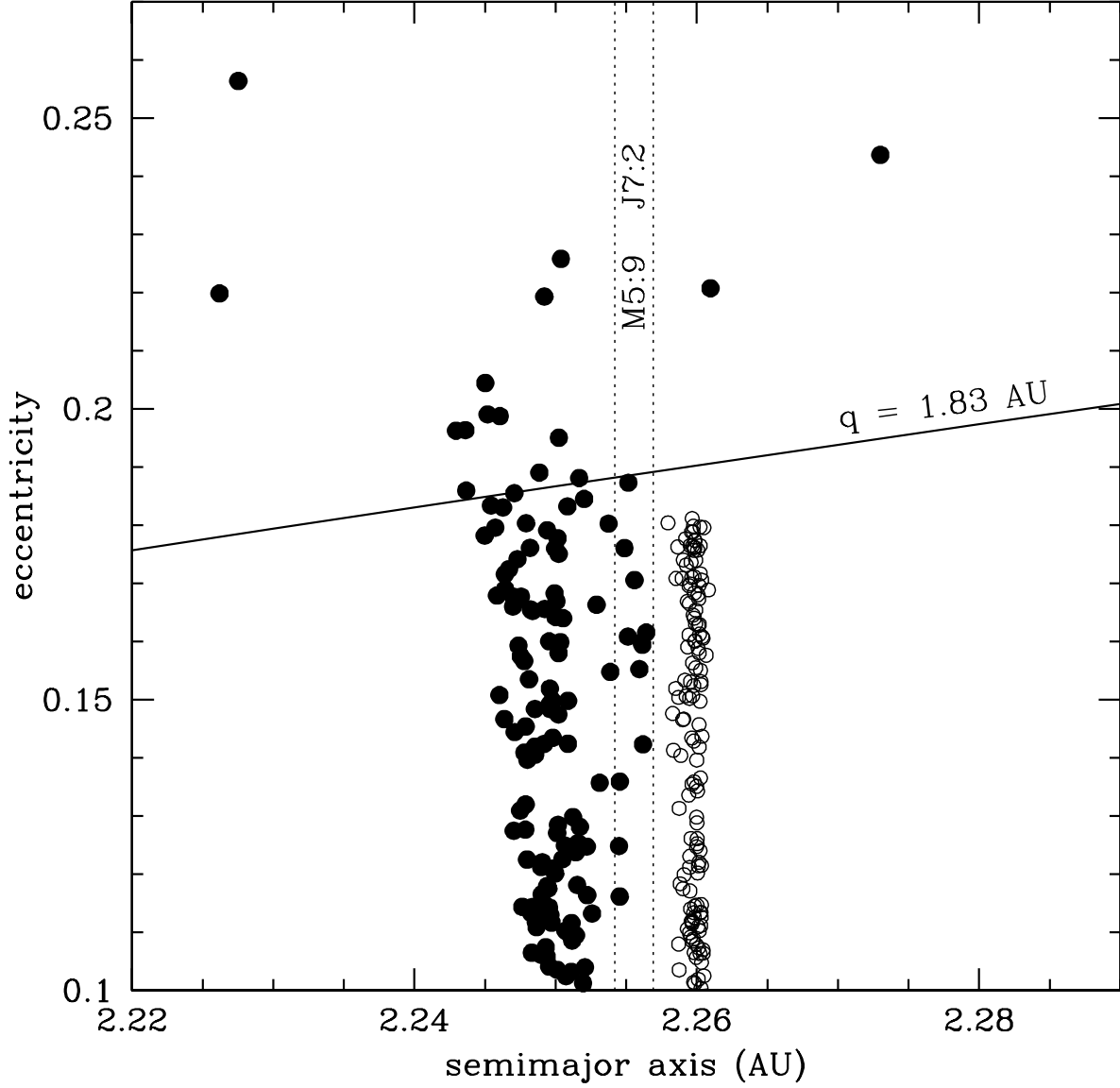
Fig. 3.— The evolution of massless test particles evolving while a constant change in semi-major axis of 10^{-4} AU/MYR is applied. The plot shows the eccentricity and semimajor axis for each of the 155 particles at the start of the integration (open symbol) and at the end of the 100 Myr integration (closed symbols). The vertical dashed lines are the location of the Jupiter 7:2 MMR and the Mars 5:9 MMR, while the horizontal dashed line represents a Mars-crossing orbit at $q = 1.83$ AU

Table 1: MIRSI observations of 1996 FG$_3$ on 2009 May 1 UT. 1996 FG$_3$ was at a heliocentric distance of $r = 1.057\ AU$, observer-centric distance of $\Delta = 0.1567\ AU$, and phase angle of $\alpha = 67.4°$; all values were constant during our observations to within the last quoted digit.

UT	Wavelength μm	Flux Jy	Flux $10^{-14}\mathrm{W/m}^2/\mu\mathrm{m}$
05:51	11.6	1.23 ± 0.03	2.75 ± 0.07
05:53	11.6	1.29 ± 0.03	2.87 ± 0.07
05:54	11.6	1.35 ± 0.03	3.01 ± 0.07
05:59	8.7	0.86 ± 0.02	3.40 ± 0.08
06:01	8.7	0.77 ± 0.02	3.06 ± 0.08
06:10	18.4	1.80 ± 0.16	1.59 ± 0.14
06:17	9.8	0.96 ± 0.04	3.00 ± 0.13
06:20	9.8	1.05 ± 0.05	3.27 ± 0.15
06:23	9.8	0.96 ± 0.04	3.01 ± 0.14
06:25	11.6	1.23 ± 0.03	2.75 ± 0.06
06:27	11.6	1.21 ± 0.03	2.69 ± 0.07
06:30	8.7	0.75 ± 0.02	2.98 ± 0.08
06:33	8.7	0.69 ± 0.02	2.74 ± 0.09
06:36	8.7	0.76 ± 0.02	3.02 ± 0.08
06:43	18.4	1.80 ± 0.16	1.59 ± 0.14
06:48	11.6	1.10 ± 0.03	2.44 ± 0.07
06:51	9.8	0.90 ± 0.05	2.80 ± 0.15

UT	Wavelength μm	Flux Jy	Flux $10^{-14}\mathrm{W/m}^2/\mu\mathrm{m}$
00:56	8.59	0.68 ± 0.01	2.95 ± 0.05
01:14	8.59	0.73 ± 0.01	2.77 ± 0.05
00:28	11.88	1.19 ± 0.02	2.53 ± 0.05
01:05	18.72	1.31 ± 0.07	1.12 ± 0.06

Table 2: VISIR observations of 1996 FG$_3$ on 2 May 2009 UT. The target was at an observer-centric distance of 0.156 AU, a heliocentric distance of 1.053 AU, and a phase angle of 69.1°. Note: the 11.88 μm flux quoted here includes the 13% smearing correction discussed in the text.

Table 3: NEATM fit results for 1996 FG$_3$. Each dataset is analyzed with and without Q-band data. Adopted final results are given in the last line. The uncertainties in the first six lines are purely statistical, whereas the last line includes systematics.

Data set	D(km)	p_V	η
MIRSI+Q	$1.95^{+0.06}_{-0.07}$	$0.036^{+0.003}_{-0.002}$	$1.67^{+0.08}_{-0.13}$
MIRSI-Q	$1.90^{+0.07}_{-0.06}$	$0.039^{+0.003}_{-0.003}$	$1.59^{+0.10}_{-0.10}$
VISIR+Q	$1.81^{+0.07}_{-0.07}$	$0.043^{+0.004}_{-0.003}$	$1.51^{+0.10}_{-0.09}$
VISIR-Q	$1.84^{+0.11}_{-0.06}$	$0.041^{+0.003}_{-0.005}$	$1.55^{+0.14}_{-0.06}$
Both+Q	$1.94^{+0.03}_{-0.06}$	$0.037^{+0.003}_{-0.001}$	$1.67^{+0.03}_{-0.08}$
Both-Q	$1.96^{+0.05}_{-0.06}$	$0.036^{+0.003}_{-0.002}$	$1.69^{+0.06}_{-0.09}$
Adopted	1.90 ± 0.28	0.039 ± 0.012	1.61 ± 0.08